Present-day strain distribution across the Minab-Zendan-Palami fault system from dense GPS transects

Michel Peyret, Y. Djamour, K. Hessami, V. Regard, O Bellier, Philippe Vernant, Marc Daignieres, H. Nankali, S. van Gorp, M. Goudarzi, et al.

Geophys. J. Int. (2009) **179,** 751–762 doi: 10.1111/j.1365-246X.2009.04321.x

Present-day strain distribution across the Minab-Zendan-Palami fault system from dense GPS transects

M. Peyret,[1] Y. Djamour,[2] K. Hessami,[3] V. Regard,[4,5,6] O. Bellier,[7] P. Vernant,[1] M. Daignières,[1] H. Nankali,[2] S. Van Gorp,[1] M. Goudarzi,[2] J. Chéry,[1] R. Bayer[1] and M. Rigoulay[1]

[1] *Université Montpellier 2, Géosciences Montpellier,* CNRS UMR-5243, 34095 *Montpellier, France. E-mail: peyret@gm.univ-montp2.fr*
[2] *National Cartographic Center (NCC), Tehran, Iran*
[3] *International Institute of Earthquake Engineering and Seismology (IIEES), Tehran, Iran*
[4] *Université de Toulouse; UPS (SVT-OMP); LMTG;* 14 *Av, Edouard Belin,* F-31400 *Toulouse, France*
[5] *CNRS; LMTG;* F-31400 *Toulouse, France*
[6] *IRD; LMTG;* F-31400 *Toulouse, France*
[7] *CEREGE (UMR CNRS–Aix-Marseille Université, IRD et Collège de France, Université P.Cézanne, Europôle de l'Arbois,* BP 80, 13545 *Aix-en-Provence Cedex* 4, *France*

Accepted 2009 July 6. Received 2009 July 2; in original form 2009 January 5

SUMMARY

The Strait of Hormuz area is a transition zone between the continental collision of the Zagros (west) and the subduction of an oceanic part of the Arabian Plate beneath the Makran wedge (east). Geology and recent GPS measurements indicate that about 15 mm yr^{-1} of relative motion in N10°E direction is accommodated by two major fault systems: (1) the NNW-trending Minab-Zendan-Palami (MZP) fault system that connects the Main Zagros Thrust (MZT) to the inner Makran thrust system and the Frontal subduction thrust and (2) the N-trending Sabzevaran-Kahnuj-Jiroft (SKJ) fault system that bounds the Jazmurian depression to the west. We use dense GPS measurements along four transects across these fault systems in order to determine the strains spatial distribution. The northern GPS transect confirms the total fault slip rates for both fault systems estimated by the tectonic analyses (about 10 and 7.3 mm yr^{-1} in N10° direction across the MZP and SKJ fault systems, respectively). For both fault systems, the elastic deformation spreads over shear zones that are several tens of kilometres wide. However, transects located close to latitude 27°N reveal a much narrower shear zone (∼10 km) for the MZP fault system. Moreover, we confirm that most of the present-day strain is transferred towards the frontal subduction thrust rather than towards the inner Makran thrusts. In order to complement this new GPS velocity field with spatially dense measurements, we processed a set of ERS radar images by the radar interferometry (InSAR) technique. We used both a 'stacking' and a 'persistant-scatterers' approach to differentiate the ground deformation signal which spatial gradient is expected to be very low, from the atmospheric signal. Results from these interferograms appear to be relatively in agreement with the GPS-determined strain distribution. Nevertheless, they confirm the absence of any superficial creep behaviour since no sharp discontinuity on interferometric phase can be noted on any interferogram. Finally, we use a purely kinematic 'block model' inversion process to calculate slip rates and locking depths for each fault system from our GPS measurements. These models suggest that the relative quiescence over the last 200 yr has certainly produced a slip deficit as high as 2 m. So, we may wonder if the MZP fault system is not late in the interseismic phase of its earthquake cycle.

Key words: Inverse theory; Satellite geodesy; Radar interferometry; Seismicity and tectonics; Transform faults.

1 INTRODUCTION

The convergence of the Arabian and Eurasian plates, geodetically estimated to about 23 mm yr^{-1} in N10°E direction in the Hormuz Strait (e.g. Vernant *et al.* 2004; Reilinger *et al.* 2006), is almost completely accommodated within the Iranian borders in the Zagros, Alborz and Kopet-Dahg mountain belts (e.g. Jackson & McKenzie 1984, 1988; Jackson *et al.* 1995). Within this tectonic

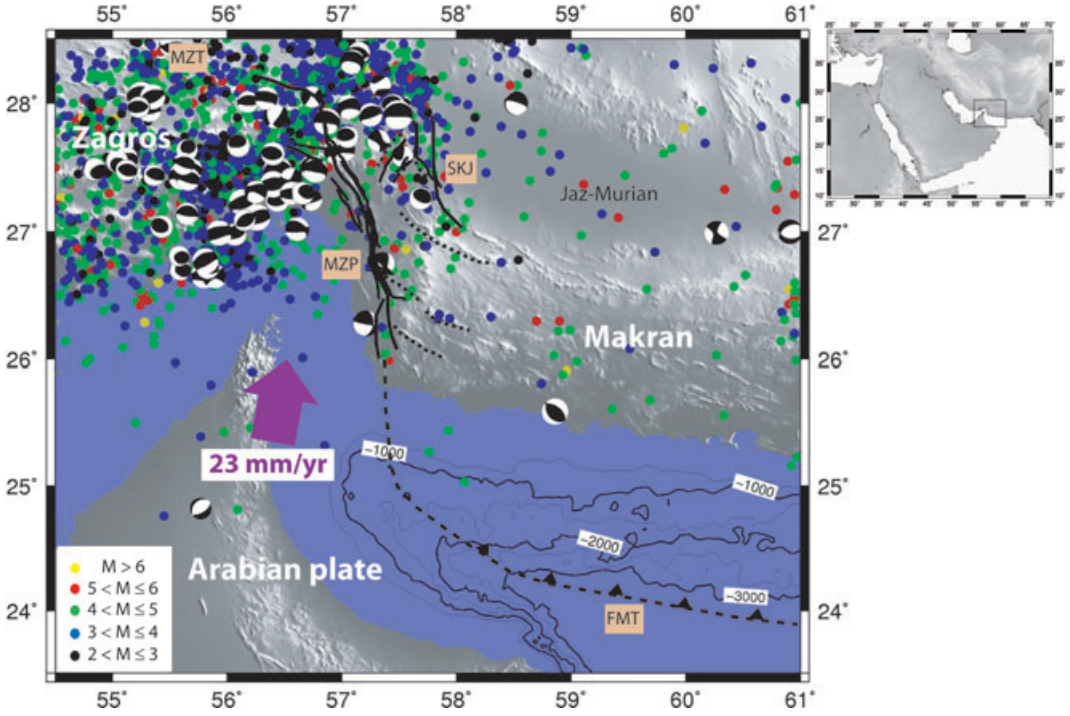

Figure 1. Simplified seismotectonic map of the transition area between the collision zone of Zagros and the subduction of an oceanic part of the Arabian Plate beneath the Makran. Inset in upper right map shows the location of the study zone. Major active faults are shown as black lines (MZT: Main Zagros Thrust, MZP: Minab-Zendan-Palami fault system, SKJ: Sabzevaran-Kahnuj-Jiroft fault system, FMT: Frontal Makran Thrust). Historical and instrumental seismicity (magnitude higher than 2.5) is from IIEES earthquake catalogue (http://www.iiees.ac.ir/english/bank/eng_databank.html). Focal mechanisms are from Harvard CMT solutions. The Arabia–Eurasia convergence rate estimated by GPS in the Strait of Hormuz is 23 mm yr^{-1} (Vernant *et al.* 2004). Background shaded digital elevation model is from SRTM data (Farr *et al.* 2007). Contour lines are in metre.

context, the Hormuz Strait is especially interesting since it is a transition zone between the continental collision of the Zagros and the subduction of an oceanic part of the Arabian Plate beneath the Makran wedge (Fig. 1). Previous GPS and geomorphic analyses revealed that two major fault systems accommodate about 15 mm yr^{-1} of deformation in N10°E direction (Regard *et al.* 2004, 2005; Bayer *et al.* 2006). The Minab-Zendan-Palami (MZP) fault system and further to the northwest, the N-trending Sabzevaran-Kahnuj-Jiroft (SKJ) fault system. The MZP fault system transfers deformation from the Zagros towards the Makran wedge, while the SKJ fault system transfers deformation northward in the Alborz and Kopet-Dahg mountain belts, via the large dextral strike-slip fault system of Nayband and Gowk (Regard *et al.* 2004, 2005). The obliquity of convergence with respect to mean fault strike, roughly trending N to N160°E, indicates a transpressive tectonic context.

Surprisingly, historical (Ambraseys & Melville 1982; Musson 2009) and instrumental seismicity (e.g. Gholamzadeh *et al.* 2009; Fig. 1), as well as microseismicity activity (Yamini-Fard *et al.* 2007), appear to be essentially limited to the Zagros domain, west of what is generally referenced as the Oman-line. East of that limit, the seismic activity is much weaker and quite distributed.

Thus, MZP and SKJ are rather rapid faults and yet, their kinematic behaviour, especially for MZP, seems to be aseismic. Hence, it is critical to map precisely the strain accommodation at the crustal scale in this area. According to geology, this strain accommodation is rather uniformly distributed over all these faults, except the Minab fault, which is supposed to act as a minor thrust fault. However, geomorphic analyses support distributed rather than localized ground-surface deformation over this wide juvenile transition area (Regard *et al.* 2004, 2005).

In order to quantify the present-day strain rate distribution, Bayer *et al.* (2006) installed a regional GPS network that covers the whole transition area from longitude 56°E to 58°E (Fig. 2). Its spatial sampling is about 1 site every 50 km. Hence, it could not address the question of detailed strain distribution within each fault system. Their velocity field is generally consistent with geologically determined fault slip rates. However, precise details of strain distribution remain unknown. Thus, we speculate that superficial creep process may be involved in this strain accommodation. Similarly, is the present-day deformation mainly accommodated by one single fault or distributed over several faults? The velocities of GHOL and SORC sites indicate a dextral strike-slip displacement of 3.1 ± 2.5 mm yr^{-1} in north-direction for the SKJ fault system (Fig. 2), whereas geology suggests as much as 5.63 ± 1.52 mm yr^{-1}. So it is important to verify whether the GPS analysis has missed some part of the elastic deformation associated with the SKJ fault system or not. Finally, from south to north, JASK, MOSH and GHOL sites have similar velocities. However, Regard *et al.* (2004, 2005) suggest that the total strain accommodated by the MZP fault system should decrease from north to south. It raises the question of whether the MZP fault system transfers a significant part of deformation within the inner Makran wedge (as stated by geology), or rather to the frontal Makran thrust.

A better understanding of the past- and present-day strain distribution over this transition zone can help to understand the seismogenic fault behaviour and to assess the seismic hazard associated to MZP and SKJ fault systems. In particular, we speculate that the

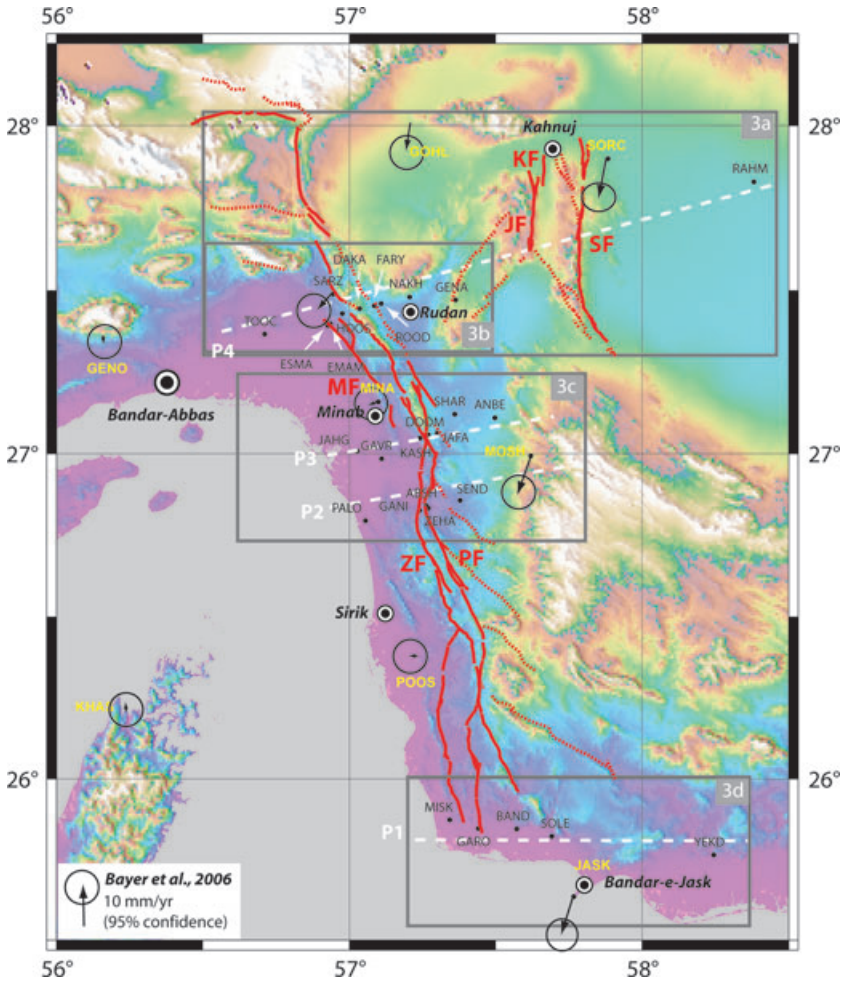

Figure 2. Localization of GPS sites. This dense network spatially samples the MZP and SKJ fault systems along four profiles: P1 along the southern coast, P2 and P3 in the central area where Minab, Zendan and Palami faults (MF, ZF and PF, respectively. Fault mapping after Regard *et al.* 2004) are very close to each other, and P4 from the Bandar-Abbas coastal plain to the Jazmurian depression via the Rudan plain. The former GPS velocity field obtained by Bayer *et al.* (2006) is depicted with black arrows. Grey boxes delimitate the areas for Fig. 3. White dotted lines indicate the location of profiles used for Fig. 4.

MZP fault system may be nearing the end of the seismic strain accumulation phase of the seismic cycle.

To address all these questions, we first summarize the basic tectonic and seismic settings of the studied area. Then we present a velocity field derived from four dense GPS profiles across the MZP and SKJ fault systems. In order to get a high-spatial density map of ground deformation, we report the results of a radar interferometric analysis (InSAR). These present-day geodetic estimations of strain accommodation are compared with long-term fault slip-rates deduced from tectonic study. Then, we use a purely kinematic block model for estimating fault slip-rates and fault locking depths from GPS velocity field.

2 TECTONIC AND SEISMIC SETTINGS

The convergence of the Arabian Plate towards Eurasia results both in a continental collision west of the Hormuz strait (Zagros), and in an oceanic subduction beneath the Makran wedge to the east (Fig. 1). This convergence rate increases eastwards to 23 mm yr^{-1} at longitude 56.5°E (McClusky *et al.* 2003; Vernant *et al.* 2004; Bayer *et al.* 2006; Masson *et al.* 2007). The Zagros NW-trending fold-and-thrust belt accommodates about 7 mm yr^{-1} of shortening, up to 10 mm yr^{-1} at its southeastern most end (Alavi 1994; Tatar *et al.* 2002; Blanc *et al.* 2003; Talebian & Jackson 2004; Vernant *et al.* 2004; Authemayou *et al.* 2006, 2009; Hessami *et al.* 2006; Masson *et al.* 2007) whereas the Makran subduction undergoes about 20 mm yr^{-1} of shortening in a N20°E-trending convergence (Vernant *et al.* 2004; Masson *et al.* 2007). Thus, the Hormuz strait area should accommodate about 10–13 mm yr^{-1} of right-lateral movement.

This Zagros–Makran transition zone has been the subject of numerous studies in geodesy, tectonics, seismology and palaeomagnetism in order to better understand its structure and its kinematics (e.g. Regard *et al.* 2008).

The EW-striking Makran belt (east of longitude 57°E) is the emerged portion of an extensive accretionary prism (Byrne & Sykes 1992; McCall 1997; Kopp *et al.* 2000). Its frontal thrust is located about 70 km seaward (Fig. 1). The onset of this subduction of an oceanic part of the Arabian Plate beneath Eurasia is estimated to Palaeogene times (Platt *et al.* 1988), while accretion started during Eocene times (Byrne & Sykes 1992). The modern accretionary prism has developed since late Miocene (Platt *et al.* 1985, 1988) and is still propagating seaward at a rate of 10 mm yr^{-1} (White 1982). Thus, this transform zone has been structured during the last 15 Myr and therefore can be considered as being immature.

The sediment thickness on top of the oceanic crust is extremely high (>6 km), and the dip angle of the subduction is extremely low (∼5°; Jacob & Quittmeyer 1979; Byrne & Sykes 1992).

Surface deformation is largely distributed over a wide zone stretching from the Hormuz strait to the Jazmurian depression (Fig. 1). However, two major fault systems within the transition domain display evidence for late Quaternary oblique reverse right-lateral slip faulting (Regard *et al.* 2004, 2005): the MZP fault system, which connects the Main Zagros Thrust (MZT) suture to the frontal Makran Thrust and the SKJ fault system. The MZP fault system, that trends N to NNW, is oblique to the Arabia–Eurasia convergence, inducing a dextral transpressive context. The Zendan fault corresponds to the main lithological boundary between Zagros and Makran. The main role of the MZP fault system is to transfer deformation from Zagros to the Makran wedge. Part of the deformation accommodated to the North by the MZP fault system is expected to be transferred further south to the inner Makran thrusts in a horsetail pattern (Regard *et al.* 2004, 2005). To the east, the N-trending SKJ fault system bounds the western side of the Jazmurian depression. This is the southern termination of the large central Iranian Nayband-Gowk strike-slip fault system. SKJ fault system transfers some motion northward to the Alborz/Kopet-Dagh convergence zone in northern Iran.

This domain has experienced two successive tectonic regimes. From upper Miocene to Pliocene, deformation was characterized by partitioning between reverse faulting and en-echelon folding. Since the upper Pliocene, a NE trending $\sigma 1$-axis transpressional regime homogeneously affects the region. No partitioning process occurs in the present-day period (Regard *et al.* 2004).

Historical and instrumental seismicity (Fig. 1) provide evidence for an aseismic behaviour for the Jazmurian depression. Nearly all of the seismicity is located within the Zagros or along the SKJ fault system. A sharp boundary (roughly running on from the Musandan peninsula and sometimes called the Oman line) exists between a region of high seismicity (to the northwest: the Zagros domain) and a region of low seismicity (to the east). On this zone, the analysis of microseismicity ($M \sim 2$) (Yamini-Fard *et al.* 2007) and Tiab earthquake aftershocks (Gholamzadeh *et al.* 2009) reveal that hypocentres depth increases northeastwards. It indicates a thrusting of the lower crust on the upper crust. Moreover, this microseismicity is mainly diffuse between the MZT and the SKJ fault systems, without any evidence of seismic behaviour for the major faults.

3 RESULTS

3.1 Velocity profiles across the MZP fault system from differential GPS

Bayer *et al.* (2006) estimated a velocity field using a GPS network spread over the Zagros–Makran transfer domain, with a mean baseline of about 50 km (Fig. 2). As stated above, this low spatial resolution network did not give evidence for the deformation behaviour of individual faults. Therefore, we decided to complement this network with four dense GPS profiles across the MZP and SKJ fault systems in order to determine their respective role in the strain accommodation.

Two main interseismic type of deformation may affect a fault. On the one hand, the upper brittle part of the fault may be blocked at depth. In that case the total elastic deformation accommodated by the fault is spread over several tens of kilometres across the fault (approximately three times the locking depth, Savage & Burford 1973). On the other hand, the fault may deform according to a superficial creep process. Then the deformation is localized along the fault itself. Hence, the strategy for determining the benchmark locations simply consisted in finding, for both sides of each fault, competent outcrops very close to it (few hundreds metres) for detecting potential superficial creep processes, and spreading the other benchmarks as evenly as possible along a profile normal to the fault with a half length of at least 50 km (i.e. approximately three average locking depth).

The northern profile (P4 in Fig. 2) runs from the coastal plain of Bandar-Abbas through the Rudan plain to the inner Jazmurian depression. It includes three sites belonging to Bayer's *et al.* network: SARZ, GENA and SORC. SARZ is located just a few metres from the Zendan fault. GHOL and SORC sites reveal elastic deformation associated with the SKJ fault system, but significantly lower (3.1 ± 2.5 mm yr^{-1}) than established by geology and geomorphology (5.70 ± 1.9 mm yr^{-1}). This discrepancy may come from the nearness of SORC to Sabzevaran fault. This is why we installed the RAHM site, about 50 km further into the Jazmurian depression.

Further to the south (south of the Minab fold, roughly at latitude 27°N), the MZP fault system is characterized by a slight change of strike and a great proximity of Zendan and Palami faults, separated in places by as less as few hundreds of metres. Profiles P3 and P2 (Fig. 2) incorporate two benchmarks from Bayer's *et al.* (2006) network: MINA and MOSH.

Finally, along the southern coast (Fig. 2, profile P1), the JASK velocity obtained by Bayer *et al.* (2006) raises a major issue. Indeed, even though Bayer *et al.* (2006) and Regard *et al.* (2005) agree on the global velocity field over this transfer zone, they disagree on the distribution and transfer of deformation. Thereby, the question of a possible localized active tectonic structure west of Jask that would accommodate about 10 mm yr^{-1} of deformation is considered, whereas fieldworks predict undetectable or totally diffuse surface deformation.

In addition, our GPS network has been designed in order to analyse the along-strike evolution of the velocity gradient across the MZP fault system from latitude 27.5°N to 25.7°N. The question is to know if a significant part of the present-day deformation is transferred within the thrusts system of the inner Makran (typically at latitudes higher than 26.5°N) or if this deformation is fully transferred by the MZP fault system to the southern offshore Frontal subduction Thrust.

All these benchmarks allow for antenna forced centreing ensuring submillimetre accuracy of the GPS antenna set up. Most of them have been drilled in sandstone or limestone blocks, but some are on concrete bases built to overcome the absence of competent boulders (Table 1). They have been measured three times (January 2005, 2006, 2008) with 48-hr-long sessions. There are three exceptions: DOOM and GANI could not be measured in 2005 due to river floods, while ZEHA was damaged between 2005 and 2006. For this latter site, the hole containing the antenna adaptor was preserved. Thus, we used it for creating a new marker in the same location. This site has been measured in 2006 and 2008 using a tripod. Its GPS time-series appears to be homogeneous over the three campaigns. We used Trimble 4000SSi receivers. The data have been processed with GAMIT/GLOBK software (Herring 2002; King & Bock 2002). This analysis includes a combination of our network with other Iranian GPS networks (Vernant *et al.* 2004; Bayer *et al.* 2006; Walpersdorf *et al.* 2006).

The velocity field derived in this study is expected to express the present-day interseismic deformation on the MZP and SKJ fault systems area. Indeed, it is *a priori* free of any transient strains

Table 1. GPS site velocities and 1σ uncertainties.

Lon	Lat	Evel	Nvel	Eσ	Nσ	Cor	Name	Comments
56.711	27.365	−2.11	−1.14	1.34	1.31	−0.007	TOOC	Concrete tile
56.927	27.392	−3.08	−4.14	1.35	1.33	−0.010	ESMA	Concrete embankment
56.936	27.398	−3.58	−4.62	1.34	1.31	−0.009	EMAM	Limestone outcrop on 4ary alluvial surface
56.977	27.429	−4.86	−6.32	1.35	1.32	−0.010	HOSS	Concrete tile
56.946	27.488	−2.48	−6.73	1.09	1.09	−0.016	SARZ	Sandstone with conglomerate
57.036	27.444	−6.19	−10.32	1.33	1.30	−0.011	DAK1	Limestone within coloured-melange unit
57.085	27.453	−3.29	−9.35	1.36	1.33	−0.012	FARY	Metamorphic rock from coloured-melange unit
57.109	27.459	−6.10	−11.35	1.35	1.32	−0.012	ROOD	Sandstone and limestone reef
57.207	27.480	−7.08	−11.37	1.35	1.32	−0.013	NAKH	Radiolarite from coloured-melange unit
57.363	27.470	−2.47	−10.31	1.06	1.00	−0.025	GENA	Coloured-melange unit
57.884	27.901	−1.58	−14.21	0.92	0.88	−0.058	SORC	Coloured-melange unit
58.382	27.831	−3.55	−17.52	1.37	1.34	−0.036	RAHM	Concrete embankment
57.027	27.009	−1.24	−1.63	1.34	1.30	−0.006	JAHG	Sandstone with shells
57.111	26.985	−5.28	−5.19	1.34	1.31	−0.007	GAVR	Sandstone with conglomerate
57.100	27.160	−5.37	−5.52	1.05	1.00	−0.015	MINA	Kheku sandstone reef
57.242	27.048	−7.08	−6.32	1.35	1.31	−0.008	KASK	Concrete tile
57.270	27.058	−8.81	−13.29	1.71	1.67	−0.011	DOOM	Concrete tile
57.301	27.063	−5.32	−11.80	1.36	1.32	−0.010	JAFA	Coloured melange block
57.360	27.121	−6.59	−11.21	1.33	1.29	−0.009	SHAR	Sandstone reef
57.497	27.110	−3.61	−13.04	1.37	1.34	−0.013	ANBE	Limestone
57.055	26.795	−2.48	−0.25	1.34	1.31	−0.005	PALO	Sandstone and conglomerates stratification
57.240	26.827	−6.10	−4.18	1.67	1.62	−0.007	GANI	Microconglomerates in Kheku sandstone
57.265	26.843	−5.88	−9.14	1.35	1.30	−0.007	ABSH	Limestone outcrop on 4ary alluvial terrace
57.270	26.833	−5.08	−12.33	1.38	1.33	−0.008	ZEHA	Limestone outcrop on 4ary alluvial terrace
57.378	26.857	−4.93	−10.28	1.36	1.31	−0.008	SEND	Limestone
57.620	26.993	−4.00	−13.23	1.02	0.96	−0.018	MOSH	Limestone within the colour-melanged complex
57.343	25.873	−2.05	−0.80	1.39	1.34	0.008	MISK	Thin limestone layer on sandstone reef
57.441	25.846	−6.20	−4.90	1.36	1.31	0.009	GARO	Thin limestone layer on sandstone reef
57.572	25.845	−8.58	−10.65	1.38	1.32	0.008	BAND	Sandstone
49.328	32.037	−2.74	−2.28	1.59	1.54	0.036	SOLE	Sandstone within Kuh-e-Deraz fold
57.767	25.636	−3.78	−12.51	1.00	0.92	0.034	JASK	Concrete pillar
58.246	25.765	−6.54	−14.68	1.39	1.31	0.009	YEKD	Sandstone

Notes: Latitude (Lat) and longitude (Lon) are given in degrees north and east, respectively. Velocities and uncertainties are given in mm yr^{-1}. Velocities are expressed with respect to fixed Arabia. Evel and Nvel are the east and north components of velocities. Eσ and Nσ are the east and north components of 1σ uncertainties. The correlation coefficient between the east and north uncertainties is also provided (Cor). The last column gives some comments on the physical characteristics of the site.

associated with the relaxation of stresses caused by large recent earthquakes.

The vertical component of the resulting velocity field is null within the 95 per cent confidence level ellipse error, except for DOOM and JASK sites. DOOM has been measured only twice, hence it is difficult to discriminate vertical displacement from measurement error (equipment or installation). By contrast, JASK site has been measured six times since 2000 and its vertical time-series reveals a constant decrease of its position with a significant acceleration since 2002. This concrete pillar located on the sea front seems to subside by about 10–20 mm yr^{-1}. This could be related to a blocked underlying subduction plane. However, none of the other sites located along the southern coast reveal any similar vertical motion. Hence, we attribute this behaviour to local subsiding effect (e.g. instability of the pillar or diagenesis effect). Nevertheless, we will see that its horizontal velocity remains coherent within the southern velocity profile.

The horizontal velocity vectors, expressed in a fixed Arabia reference frame, are presented in Table 1 and Figs 3 and 4. Velocities of common sites are in agreement with Bayer *et al.* (2006) results. Indeed, additional sites in the far-field (YEKD, ANBE and RHAM) confirm the uniform N10°E-trending deformation accommodated by MZP and SKJ fault systems. Along the western coast, sites MISK, PALO, JAHG and TOOC have very low velocities with respect to fixed Arabia, indicating that they belong to the Arabian Plate. Moreover, this new velocity field clearly demonstrates that interseismic surface deformation across the MZP and SKJ fault systems is diffuse. Indeed, none of the benchmarks pairs located close to any fault display any sharp discontinuity of the horizontal velocity. Furthermore, the strain field is spread over several tens of kilometres, centred on the mean location of each fault system. Thus, it is difficult to discriminate the activity of the distinct faults within each fault systems according to the measured ground deformation.

The differential of about 15 mm yr^{-1} between east and west is accommodated over about 50, 10 and 50 km, along the Jask (P1), Minab-Sirik (P2 and P3) and Roudan (P4) profiles, respectively. The fault-parallel velocity gradients across the MZP fault system are symmetrical about a location close to the mean trace of the mapped faults. As to the fault-perpendicular component, the far-field gradient across the MZP fault system displays about 3 mm yr^{-1} of compression, uniformly from south to north. All profiles highlight a similar evolution of this perpendicular component within the near-field, which corresponds to an increase, then decrease of compression from west to east. This is particularly notable on profiles P1 and P4.

3.2 InSAR analysis

Whatever spatial resolution is achieved by a GPS network, measurements are still localized and sparse. Thus, it always remains the

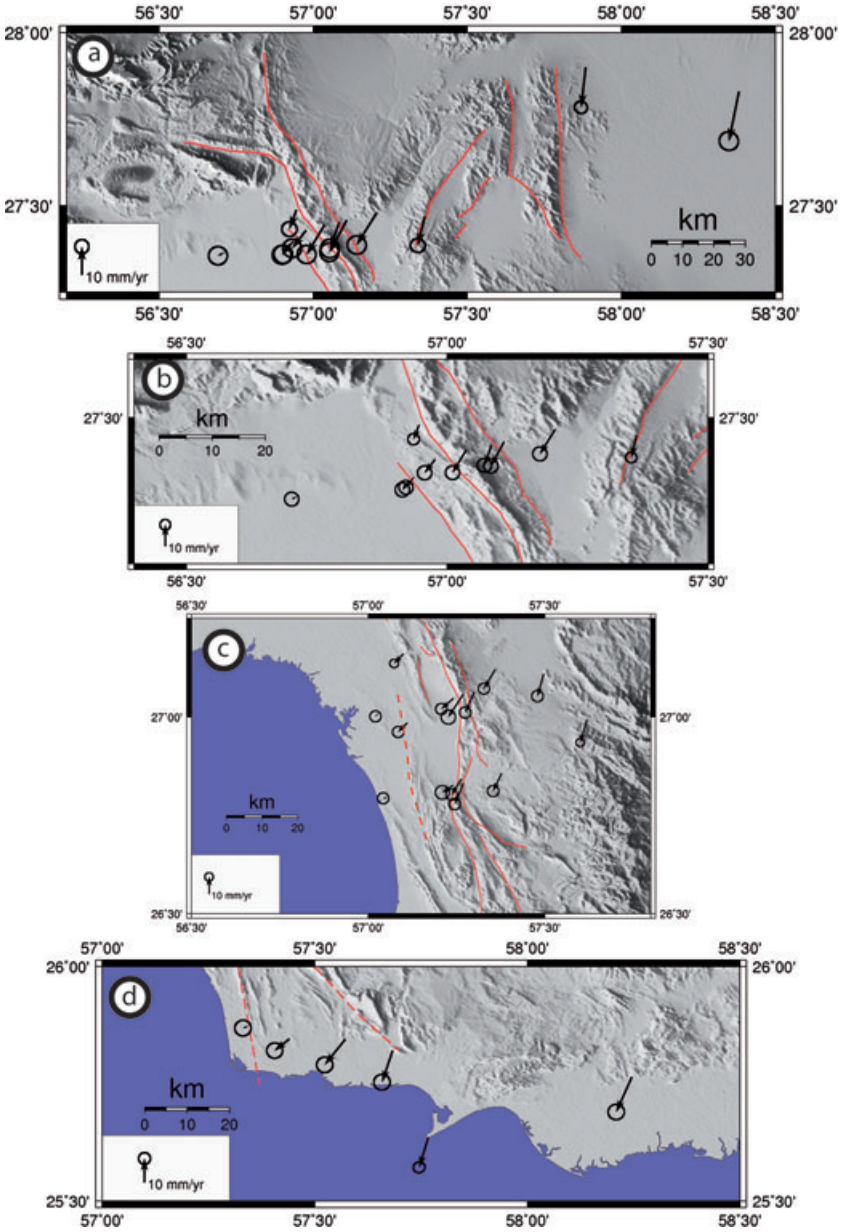

Figure 3. GPS horizontal velocities with respect to fixed Arabia, and their 95 per cent confidence ellipses. Maps (a) and (b) correspond to the northern frame in Fig. 2, map (c) to the central frame and map (d) to the southern frame. Faults traces are mapped in red. Dotted lines are used for less obvious active fault location. This is particularly the case on frame (c). The western dotted line, located about 10 km west of the MZP fault system, is mainly suggested by the relative velocity change between JAHG and GAVR sites (see Fig. 4, profile P3). However, this assumption is not really supported by field observations.

question of possible missing motion. This is the case in our GPS study, both longitudinally (what happens between our profiles?) and laterally.

InSAR (e.g. Massonnet & Feigl 1998; Bürgmann *et al.* 2000) is a remote sensing technique which allows mapping ground deformation with a high-spatial density (decametric) and a high precision (subcentimetre along the satellite line of sight). The main requirement is the conservation of geometrical and physical properties of homologous pixels between the two satellite acquisitions (Zebker & Villasenor 1992). From this point of view, the Zagros–Makran transition zone is favourable since it is an arid region with poor vegetation coverage. However, InSAR measures ground deformation projected along the satellite line of sight (LOS), which is unfortunately, essentially oriented eastward and up. Therefore, InSAR is almost blind to ground deformation associated with north-trending faults. The horizontal velocity change across the MZP fault system, estimated to about 15 mm yr^{-1} in N10°E direction, projects onto the ERS or Envisat satellite LOS at about 0.1 cm yr^{-1}, that is to say 1/28 of fringe yr^{-1}. At most this will produce about one fourth of a fringe in interferograms spanning about 7 yr (duration of ERS or Envisat archives). Such a small change in phase delay may be detectable in case of sharp localization (superficial creep process), whereas it is almost impossible to detect in case of diffuse deformation.

We processed 18 ERS raw data, in descending orbit, at latitude of Minab. The interferometric processing was achieved with Roi_Pac software (Rosen *et al.* 2004). Interferometric coherence is good everywhere (even for long time-intervals), except along the coastal

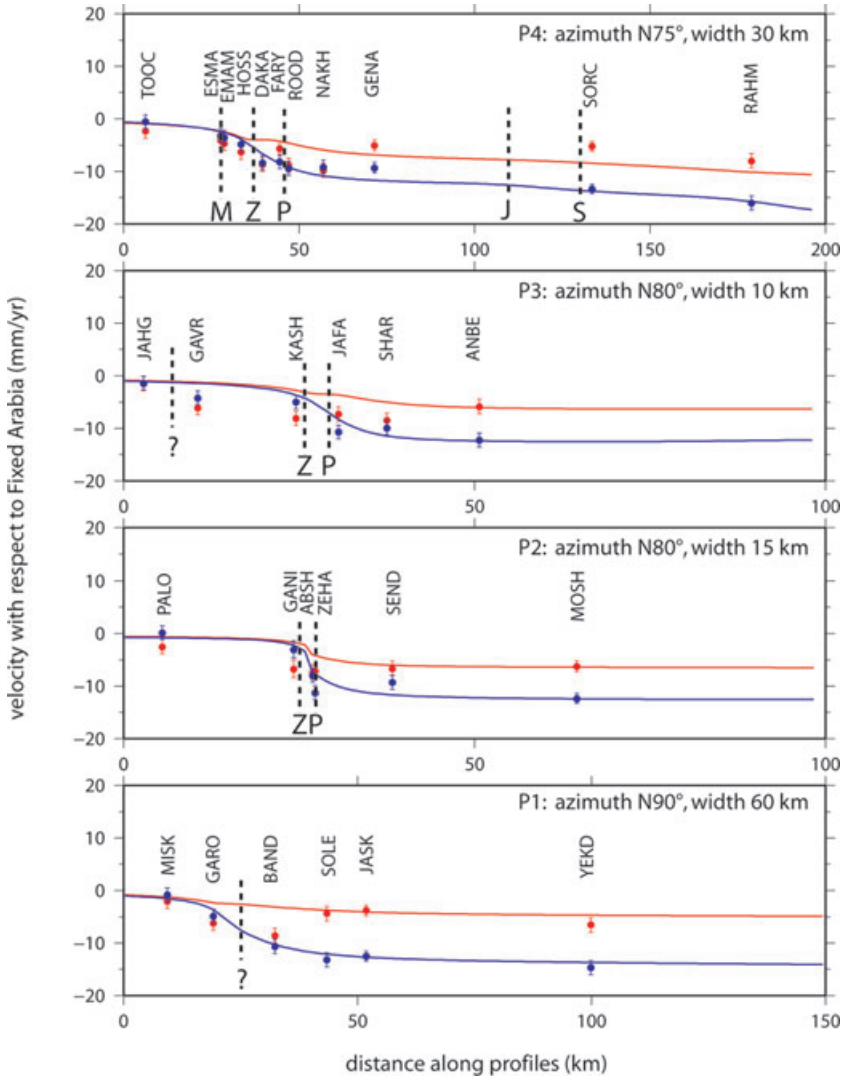

Figure 4. Projection of horizontal velocity vectors onto the profiles mapped on Fig. 2. Profiles are roughly perpendicular to the local faults strike. The fault-parallel component is in blue, and the component perpendicular to the fault is in red. GPS observations are displayed with circles and error-bars. The simulation from our preferred model of slip distribution along MZP and SKJ fault systems is represented with solid curves. Fault locations are specified with dotted black lines.

plain where one can find palm trees plantations and agricultural areas.

The main source of phase delay for all the processed interferograms is the relative change in atmospheric conditions. This effect adds spatially coherent noise on phase at spatial scales ranging from several hundreds metres to tens of kilometres. The mean amplitude of these artefacts is about one fringe. The aspect of this contribution is that it becomes difficult to detect small distributed ground-deformation gradient (typically 10^{-3} fringe km^{-1}) simply by a cross-analysis of this collection of interferograms. By contrast, the unmodelled atmospheric noise does not mask any possible phase discontinuity (or high gradient, typically 10^{-1} fringe km^{-1}) due to surface creep process on a fault. Thus, since such phase discontinuity has not been found on any interferogram and any fault segment (whatever its orientation with respect to the satellite LOS, which changes significantly over the study area), it is possible to exclude superficial creep process as a possible fault behaviour in this area. This is in agreement with our GPS velocity field, and geology or geomorphology assessment. Likewise, the lack of microseismicity argues in favour of elastic deformation rather than creeping.

In order to try to extract the elastic interseismic ground deformation from the InSAR data, we implemented the stacking approach (Sandwell & Price 1998) and a persistent-scatterers InSAR (PS-InSAR) technique (Hooper 2004, 2006, 2007). On the one hand, since atmospheric contribution to phase delay is random from one epoch to another, the stacking process statistically reduces the atmospheric signature while increasing the permanent ground-deformation signature. On the other hand, PS-InSAR strategy consists of first selecting pixels with steady phase-behaviour over the whole set of interferograms, and then discriminating gradual changes (e.g. ground deformation) from single-epoch changes (e.g. atmosphere) in the analysis of the time-series of interferometric phase.

We stacked six independent interferograms each spanning at least 3 yr, and having a perpendicular baseline smaller than 100 m in order to limit the geometric decorrelation. The cumulated time is 24.5 yr. Thus, the expected interferometric phase difference across

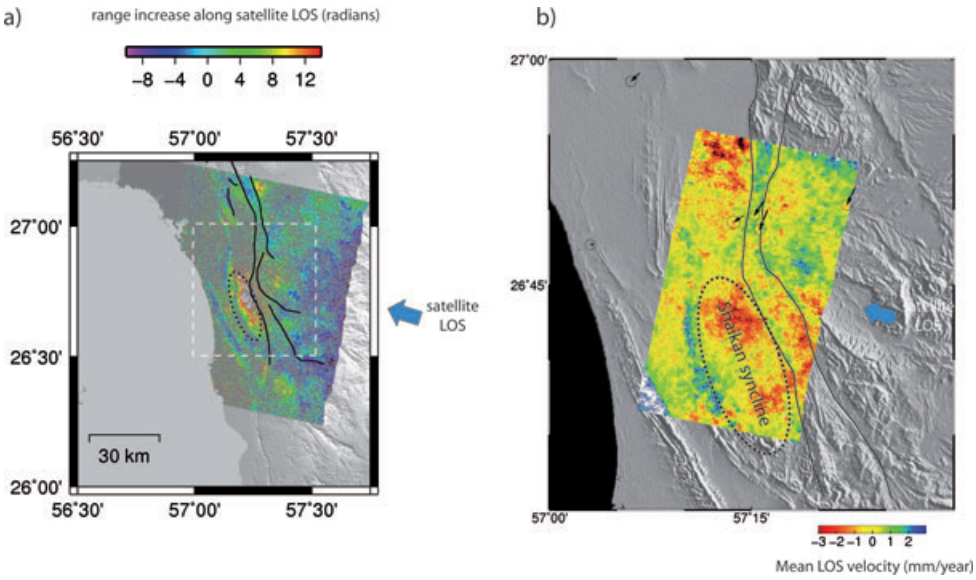

Figure 5. (a) Stacked interferogram spanning a cumulative time interval equal to 24.5 yr. The western area of the MZP fault system appears to move away from the satellite, with respect to the eastern area. The mean phase difference between East and West is about 9 radians (that is to say 4 cm along the satellite LOS). These values are consistent with the present-day tectonic loading of that region. However, this interferogram is rather noisy (pixels with low coherency have been masked).

the MZP fault system is about 1 fringe. The stacked interferogram is presented in Fig. 5(a). The western area of the MZP fault system appears to move away from the satellite, with respect to the eastern area. The mean phase difference between east and west is about 9 radians [that is 1 fringe and a half, or 4 cm (1.7 mm yr^{-1}) along the satellite LOS]. These values are consistent with the expected tectonic loading of that region which is supposed to project onto the satellite LOS to about 1 mm yr^{-1}. However, this interferogram is rather noisy (pixels with low coherency have been masked). Moreover, the global fringe pattern does not differ significantly from a linear trend that could also be due to orbital uncertainties. Finally, localized atmospheric residues are still likely present. This is probably the case to the north (phase discontinuities across Zendan and Palami faults) and over the Shaikan syncline (Fig. 5) that borders the Zendan fault to the west at latitude 26°40′N. The northern phase discontinuity is in contradiction with the expected dextral ground motion, and thus must probably be explained by atmospheric delay. By contrast, we may wonder whether the range increase located on the Shaikan syncline does not express a local subsidence linked to reverse faulting. In any case, the number of independent interferograms available for stacking is too small for completely discriminating ground-displacement from atmospheric effects.

The complete set of radar images has also been processed in a PS-InSAR approach with Stamps software (Hooper 2004, 2006). The resulting mean velocity field (Fig. 5b) does not differ significantly from the stacked interferogram. The coastal area west of the MZP fault system appears to move away from the satellite relative to the eastern area by less than 2 mm yr^{-1}. Once again, the question of the range increase for the Shaikan syncline is posed, even though this range increase seems to affect other large zones to the northwest and southeast. The likeliest interpretation involves non-modelled atmospheric contributions. However, any ground-deformation origin cannot be definitely ruled out.

All these radar analyses agree on the diffuse characteristic of the ground deformation. A similar conclusion has been drawn from a small set of interferograms over the Jask area.

4 DISCUSSION

4.1 Geology versus geodesy

Combined analysis of geological and geodesy measurements allows for estimating the time dependence in fault slip rate. This dependency may have implications in the earthquake cycle. Within a fault system, it may also express a possible shift of localized deformation from one structure to another.

On the one hand, geology estimates the sense of motion from striations on fault planes (Regard *et al.* 2004) and the slip-rates by dating landform markers offsets (Regard *et al.* 2005). These data provide long-term rate average with limited temporal resolution of instantaneous slip rate. On the other hand, geodesy-based techniques map present-day instantaneous deformation. Contrary to geology, which derives fault slip rate directly from displacement observed in upper crust faults, geodesy enables to infer fault slip rate from far-field block motion. Thus, in the eventuality that slip-rate averages balance far-field loading, we present here a comparison between fault-slip rates on MZP and SKJ fault systems estimated either by geomorphic (Regard *et al.* 2005) or GPS velocity field analyses (Table 2).

First of all, let us note that GPS and InSAR velocity fields reinforce the diffuse aspect of surface deformation as stated by geology. The whole deformation accommodation cannot be assigned to one single upper-crust fault. However, we may consider that the Minab, Zendan and Palami subparallel faults are the surface expression of a single deep flower-structure (Regard *et al.* 2004, 2008).

In order to estimate the fault-slip rate from far-field loading, we consider pairs of GPS sites that are supposed to encompass the total elastic deformation associated with the MZP and the SKJ fault systems. Indeed, it is not possible to discriminate the role of each fault belonging to one fault system since their respective areas of elastic deformation overlap. Hence, for the MZP fault system we selected from south to north the following pairs: MISK-YEKD, PALO-MOSH, JAHG-ANBE and TOOC-GENA. The main uncertainty lies in the choice of GENA. Indeed, this site is likely

Table 2. Comparison between fault slip rates (in North and East direction, expressed in mm yr^{-1}) and azimuth (in degrees) estimated from geology and geomorphology (Table 3 from Regard *et al.* 2005), and our GPS velocity field.

$-dN$ (mm yr^{-1}) $-dE$ (mm yr^{-1}) Az (°)	Geology	Geodesy (southern, central and northern profiles)		
Total MZP	7.22 ± 2.16	*YEKD wrt fixed Arabia*	*mean ANBE and MOSH wrt fixed Arabia*	*GENA wrt fixed Arabia*
	1.38 ± 3.00	14.68 ± 1.31	13.14 ± 1.27	10.31 ± 1.00
	10.8 ± 24.0	6.54 ± 1.39	3.80 ± 1.27	2.47 ± 1.06
	or	24 ± 5	16 ± 5	13 ± 5
	5.41 ± 1.75	*MISK-YEKD*	*mean JAHG-ANBE and PALO- MOSH*	*TOOC-GENA*
	1.29 ± 2.41	13.88 ± 2.65	12.20 ± 2.46	9.17 ± 2.31
	13.4 ± 25.9	4.49 ± 2.78	1.95 ± 2.54	0.36 ± 2.40
		18 ± 10	9 ± 11	3 ± 14
Total SKJ	5.63 ± 1.52			*GENA-RAHM*
	0.87 ± 1.15			7.21 ± 2.34
	8.8 ± 11.9			1.08 ± 2.41
				9 ± 18
Total MZP + SKJ	12.85 ± 3.68	*YEKD wrt fixed Arabia*	*mean ANBE and MOSH wrt fixed Arabia*	*RAHM wrt fixed Arabia*
	2.25 ± 4.15	14.68 ± 1.31	13.14 ± 1.27	17.52 ± 1.34
	9.9 ± 18.7	6.54 ± 1.39	3.80 ± 1.27	3.55 ± 1.37
	or	24 ± 5	16 ± 5	11 ± 5
	11.04 ± 3.27	*MISK-YEKD*	*mean JAHG-ANBE and PALO- MOSH*	*TOOC-RAHM*
	2.17 ± 3.56	13.88 ± 2.65	12.20 ± 2.46	16.38 ± 2.65
	11.1 ± 18.8	4.49 ± 2.78	1.95 ± 2.54	1.44 ± 2.71
		18 ± 10	9 ± 11	5 ± 10

Notes: The comparison is made for both MZP and SKJ fault systems, each being taken as a whole. Each GPS site pair is supposed to encompass the complete elastic deformation of a fault system and we assume that fault displacement sums to far-field block motion on average. We also provide elastic deformation estimates with respect to Arabia rather than the western most GPS site on each profile. Geologically and geodetically determined fault slip rates are in good agreement within the error bars. However, contrary to the idea that a significant part of deformation is transferred within the inner Makran, geodesy suggests that this deformation is essentially transferred towards the frontal Makran thrust. Indeed, almost the total amount of deformation found between TOOC and RAHM (northern profile) is still present between MISK and YEKD (southern profile).

subject to elastic deformation associated both to MZP and SKJ fault systems. This uncertainty also affects the elastic deformation estimation of SKJ fault system with GENA-RAHM pair, but not the whole elastic deformation across MZP and SKJ fault systems estimated from TOOC-RAHM pair.

The total amount of strain accommodated by both fault systems estimated either by geology or geodesy is consistent within the measurement uncertainty. The GENA-RAHM pair estimates the specific contribution of the SKJ fault system to 7.21 ± 2.34 and 1.08 ± 2.41 mm yr^{-1} in north and east component, respectively. This is in close agreement with the geologically determined fault slip-rate: 5.63 ± 1.52 and 0.87 ± 1.15 mm yr^{-1}, respectively. It is notable that extending the domain of GPS measurement about 50 km eastward within the Jazmurian depression allowed to encompass about 3 mm yr^{-1} of elastic deformation that were missing in Bayer *et al.* (2006) study. Consequently, geodetic measurements are very consistent with the geological results when considering the northern profile (TOOC-GENA pair or GENA with respect to Arabia). GPS confirms that there is no short-term (Holocene) variation in fault loading rate.

However, geomorphic analysis predicted that a significant part of the deformation would be transferred more to the south within the inner-Makran fold and thrust belt (Regard *et al.* 2005, 2006). Thus, JAHG-ANBE, ANBE-MOSH and even more MISK-YEKD should exhibit strain rates lower than established by TOOC-GENA. Surprisingly, this is not the case. Quite the contrary, geodesy tends to indicate that not only the northern deformation accommodated by the MZP fault system is still present even at the latitude of Jask, but also some part of the SKJ fault system deformation is transferred more to the south along the MZP fault system. Only a small part of the deformation accommodated by the SKJ fault system seems to be transferred towards the southeast, south of the Jazmurian depression. This discrepancy addresses the issue of knowing whether a significant part of the deformation is transferred within the Makran accretionary wedge as proposed from the tectonics study (Regard *et al.* 2004, 2005), or if this deformation is transferred to the Makran Trench located off the coast, as shown by our current geodetic results. This difference may be explained by: (1) a time-evolution of this transform zone towards a more mature state where strain distribution becomes more localized. However, such an evolution is likely to occur on a quite longer term (typically a few Ma) and (2) a possible episodic model for the accretion of the Makran wedge (Gutscher *et al.* 1996). Such a model suggests episodic flip of deformation from the inner wedge to its front and conversely, thus resolving the apparent discrepancy between geology and geodesy measurements.

Finally, the four velocity profiles (especially the fault-parallel component) are symmetrical with respect to the mean trace of Zendan and Palami faults. This confirms their predominant role in strain accommodation as stated by geology. The influence of Minab fault seems to be minor in the northern profile. However, on profiles 2 and 3, we may wonder whether the velocity differential between PALO and GANI, but over all, between JAHG and GAVR, do not express the existence of an active segment about 20 km west of Zendan and Palami faults, in approximate northward extension of the Minab fault.

4.2 Fault slip model from GPS

Several techniques of inversion may be used for estimating the slip-rate distribution along a fault as well as the corresponding locking depth from ground-surface measurements of interseismic strain (e.g. Matsu'ura *et al.* 1986; Meade & Hager 1999; McCaffrey 2002).

We run the 'defnode' software (McCaffrey 1995) which allows for solving independently rigid blocks rotations and plate locking parameters in a pure kinematic framework, implying that information about the rheology of the upper-crust is not necessary. For instance, we do not take into account any vertical seismic velocity structure like the one provided by Yamini-Fard *et al.* (2007). Let us just note that the symmetry of strain-gradients along all the profiles rules out any significant lateral heterogeneities of rheology. A similar numerical modelling allowed Bayer *et al.* (2006) to estimate the locking depth at about 15 km, with a strike-slip rate of 15 mm yr^{-1} for the MZP fault system with about 6 mm yr^{-1} of shortening (N160°-trending), the right-lateral strike-slip rate being estimated to 3 mm yr^{-1} for the SKJ fault system.

In this numerical modelling, we defined six blocks (Arabian Plate, North and South Zagros separated by the Kazerun fault, Central Iranian block, Lut block and the Makran wedge) bordered by the main fault systems (Fig. 6). These blocks are supposed to be rigid. The validity of such an assumption is checked afterwards by controlling the rms between measured and predicted velocity field within each block. Then, active faults are defined at the interface of adjacent blocks. This implies a very simple geometrical definition of each fault. We could consider that reducing the MZP fault system to one single fault is improper; however the likely flower structure allows us to assimilate the whole fault system to one single deep fault. Three main faults have been defined: MZP, SKJ and the frontal Makran thurst (FMT). The dip angle for FMT is set to 5° northward (Byrne & Sykes 1992; Carbon 1996). For both MZP and SKJ, we impose an eastward dipping angle, which is close to verticality in the upper crust, and then decreases to a value of 10° at depth 20 km. This geometry is suggested by the deeper connection of these faults with the subduction plane. Once blocks and faults have been defined, several parameters may be either imposed or let free. The main parameters are the Euler poles associated to each block rotation with respect to fixed Arabia, and the *a priori* coupling distribution along the fault patches. In this study, Euler poles are always re-estimated by the inversion process.

At first, we simply imposed that coupling decreases along dip, then we proceeded to several trial-errors adjustments in order to improve rms along the four GPS-profiles. The various models we obtained do not differ significantly, whatever *a priori* fault geometry or coupling constrains were used. However, we needed to impose a lower locking depth close to profiles 2 and 3 in order to better simulate the local high spatial frequency of the velocity gradient. Our preferred model is presented in Figs 4 and 6. The normalized rms between observed and simulated velocity vectors within each block range from 0.9 to 1.8 mm yr^{-1}. This is below the measurement error (Fig. 6c). Hence, we consider that the rigid-block assumption is valid. The mean strike-slip rate estimated for the MZP (resp. SKJ) fault system is 12 mm yr^{-1} (respectively 7 mm yr^{-1}), with 5 mm yr^{-1} of shortening (respectively 2 mm yr^{-1}). The normalized rms for profiles P1–P4 are 1.6, 1.6, 2.2 and 1.9 mm yr^{-1}, respectively. However, the rms are quite better for the along-strike component (blue in Fig. 4) than for the perpendicular component (red in Fig. 4). Their mean values are 1.4 and 3.0 mm yr^{-1}, respectively. This discrepancy (notable on the residual velocity map, Fig. 6c) may be explained by some depth partitioning due to the change of strength between upper and lower crust. Strike-slip mechanisms would occur shallower than about 15 km, while reverse faulting would occur deeper. Therefore, our model would be more sensitive to shallow slip on faults. Another explanation could be that the lateral complexity of the fault system segmentation has probably been oversimplified in our models. At last, we may invoke some inelastic behaviour

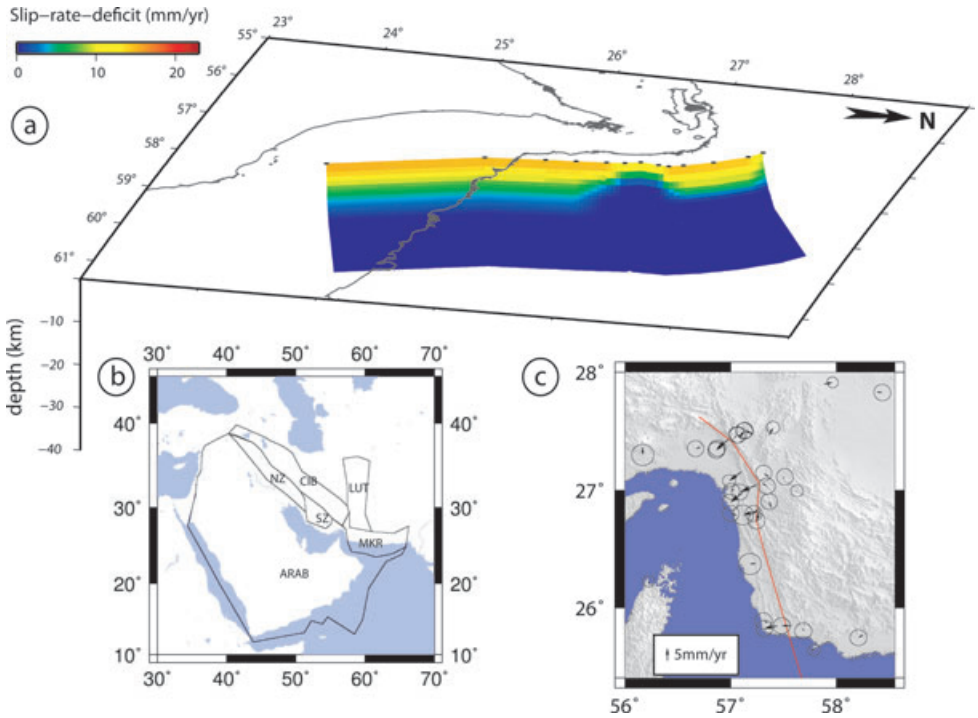

Figure 6. (a) Slip-rate deficit distribution along a simple geometrical model of MZP and SKJ faults systems. Black circles on surface are the nodes of our model. Dip angles towards east are steep close to the surface (85°) then decrease with depth. The mean slip-rate for MZP is about 15 mm yr^{-1}, and 7 mm yr^{-1} for SJ. The MZP locking depth is about 15 km except close to profiles P2 and P3 where it reaches a value as low as 2 km. The locking depth of SJ is much deeper (around 30 km). (b) Map of the rigid blocks (ARAB: Arabian Plate, NZ: North Zagros block, SZ: South Zagros block, CIB: Central Iranian block, MKR: Makran block, LUT: Lut block). (c) Map of the residual velocities between GPS velocities and velocities predicted by our model.

due to the poorly consolidated uppermost layer. Anyway, the main features of the strain gradients are respected, and whatever model is considered as long as the rms remain below some reasonable threshold, the along-strike profile of the MZP locking depth looks like in Fig. 6. The coupling parameter becomes zero roughly at depth 8 km, except close to latitude 27°N where the locking depth is estimated to less than 3 km. Nevertheless, let us note that the small number of GPS markers within each profile, associated with some poorly constrained velocity vectors (GANI, ZEHA and DOOM for profiles P2 and P3) only permit to get a rough spatial resolution (few kilometres downdip) of the slip distribution at depth.

4.3 Seismic hazard assessment

The lack of seismicity along the MZP fault system associated with a high geodetic strain requires to be understood in order to assess the seismic hazard on that region. Seismologic, geological and geodetic findings allow to rule out the presence of any superficial creep process. The precedent comparison between geodetically and geologically determined slip rates indicates that they certainly remained relatively constant in the recent geologic past. The only discrepancy between geology and geodesy relates to the role of the MZP fault system in transferring deformation either within the thrusts system of the inner Makran wedge, or more to the south towards the frontal Makran thrust. This difference is of major importance since geodesy suggests a significant higher elastic strain accumulation along the MZP fault system. However, the relative quiescence over (at least) the last 200 yr has certainly produced a slip deficit as high as 2 m. Since the locking depth estimated on the MZP is about 8 km, a rupture over a 30-km-long segment is likely to produce a $M_w \sim 6.8$ earthquake (using a shear modulus of 30 GPa).

The relationship between the tectonic loading rate and seismic activity is often complex. The preceding analysis is purely kinematic. Slip is specified along the fault rather than derived from dynamic principles. It would be valuable to estimate a basic friction law for the MZP and SKJ fault systems. Both, the lack of seismicity and the likely decoupling along the subduction plane suggest a low coefficient of friction. Furthermore, we cannot rule out that a significant part of this strain accumulation may be released by microseismicity ($M \sim 2$). Nevertheless, it is likely that the MZP fault system is late in the interseismic phase of its earthquake cycle. An earthquake with magnitude up to 7 is probably pending along the southern part of the MZP fault system.

5 CONCLUSIONS

Making the former regional GPS network processed by Bayer *et al.* (2006) denser over the MZP and SKJ fault systems, we have been able to confirm the main diffuse and elastic characteristics of the strain accumulation across this transform area. For each fault systems, the shear zone is about 50 km wide. However, this width decreases significantly at latitudes of profiles P3 and P4, where Zendan and Palami faults are very close from each other. Assuming the MZP fault system is a flower-structure with a single main fault at depth, the inversion of the GPS velocity field yields to a longitudinally varying locking depth roughly ranging from 8 to less than 3 km.

Both GPS and InSAR, as well as seismology, argue against the presence of any superficial creep mechanism on any fault, even though the locking depth estimated for profiles P3 and P4 is shallow. The strain gradient profiles are roughly centred on Zendan and Palami fault traces, revealing their major role in strain accommodation. By contrast, the Minab fault plays a minor role as stated by profile P4. However, mid-latitude profiles suggest the likely occurrence of a western minor active segment running south from the Minab Fault. This remains to be confirmed by additional measurement in the future.

The total elastic strain accommodated separately by MZP and SKJ fault systems and geodetically or geologically estimated are very consistent for the northern part of the studied zone. However, they differ to the south. Geology suggests that a significant part of strain is transferred within the inner thrusts system of the Makran wedge, whereas our GPS velocity field establishes that about 75 per cent of the strain accommodated on the northern profile by MZP and SKJ fault systems is still accommodated within a 50 km wide shear zone at latitude of Jask. This tends to prove that most of the present-day deformation is transferred to the frontal Makran thrust.

This strain localization on the MZP fault system, without transfer within the inner Makran, associated to the lack of historical and instrumental seismicity southeast of the Oman line, indicates that about 2 m of elastic strain has probably been accumulated for the last two centuries. It suggests that the MZP fault system is likely at the end of its interseismic recurrence cycle. Hence, we claim that seismic hazard on this zone is high, and that an earthquake of $M \sim 7$ is pending.

ACKNOWLEDGMENTS

We acknowledge support from European Space Agency for ERS images. We thank IIEES and NCC for fieldwork assistance. Fault mapping was done thanks to SPOT images that were provided thanks to the ISIS program (© CNES 1999–2003, distribution SPOT images S.A.). We thank R. McCaffrey for permitting the use of 'defnode' software. We thank A. Hooper for permitting the use of 'Stamps' software.

REFERENCES

Alavi, M., 1994. Tectonics of the Zagros orogenic belt of Iran: new data and interpretation, *Tectonophysics,* **229,** 211–238.

Ambraseys, N. & Melville, C., 1982. *A History of Persian Earthquakes,* Cambridge Univ. Press, Cambridge, UK.

Authemayou, C., Chardon, D., Bellier, O., Malekzadeh, Z., Shabanian, E. & Abbassi, M., 2006. Late Cenozoic partitioning of oblique plate convergence in the Zagros fold-and-thrust belt (Iran), *Tectonics,* **25,** TC3002, doi:10.1029/2005TC001860.

Authemayou, C. *et al.,* 2009. Quaternary slip-rates of the Kazerun and the Main Recent Faults: active strike-slip partitioning in the Zagros fold-and-thrust belt, *Geophys. J. Int.,* **178**(1), 524–540, doi:10.1111/j.1365-246X.2009.04191.x.

Bayer, R. *et al.,* 2006. Active deformation in Zagros-Makran transition zone inferred from GPS measurements, *Geophys. J. Int.,* **165,** 373–381.

Blanc, E.J.-P., Allen, M.B., Inger, S. & Hassani, H., 2003. Structural styles in the Zagros Simple Folded Zone, Iran, *J. Geol. Soc. Lond.,* **160,** 401–412.

Bürgmann, R., Rosen, P.A. & Fielding, E.J, 2000. Synthetic Aperture Radar Interferometry to measure Earth's surface topography and its deformation, *Ann. Rev. Earth planet. Sci.,* **28,** 169–209.

Byrne, D.E. & Sykes, L.R., 1992. Great thrust earthquakes and aseismic slip along the plate boundary of the Makran subduction zone, *J. geophys. Res.,* **97**(B1), 449–478.

Carbon, D., 1996. Tectonique post-obduction des montagnes d'Oman dans le cadre de la convergence Arabie-Iran, *Thèse*, Université Montpellier 2.

Farr, T.G. *et al.,* 2007. The Shuttle Radar Topography Mission, *Rev. Geophys.,* **45,** RG2004, doi:10.1029/2005RG000183.

Gholamzadeh, A., Yamini-Fard, F., Hessami, K. & Tatar, M., 2009. The February 28, 2006 Tiab earthquake, Mw 6.0: implications for tectonics of the transition between the Zagros continental collision and the Makran subduction zone, *J. Geodyn.,* **47,** 280–287.

Gutscher, M.A., Kukowski, N., Malavieille, J. & Lallemand, S., 1996. Cyclical behavior of thrust wedges: insights from high basal friction sandbox experiments, *Geology,* **24**(2), 135–138.

Hessami, K., Nilforoushan, F. & Talbot, C.J., 2006. Active deformation within the Zagros Mountains deduced from GPS measurements, *J. Geol. Soc.,* **163**(1), 143–148.

Herring, T.A., 2002. GLOBK: Global Kalman Filter VLBI and GPS analysis program, v. 10.0., Mass. Inst. of Technol., Cambridge.

Hooper, A., Zebker, H., Segall, P. & Kampes, B., 2004. A new method for measuring ground deformation on volcanoes and other natural terrains using InSAR persistent scatterers, *Geophys. Res. Lett.,* **31**(23), doi:10.1029/2004GL021737.

Hooper, A., Segall, P. & Zebker, H., 2007. Persistent scatterers InSAR for crustal deformation analysis, with application to Volcan Alcedo, Galapagos, *J. geophys. Res.,* **112,** B07407, doi:10.1029/2006JB004763.

Hooper, A.J., 2006. Persistant scatterer radar interferometry for crustal deformation studies and modelling of volcanic deformation, *PhD thesis*, Stanford University.

Jackson, J.A. & McKenzie, D.P., 1984. Active tectonics of the Alpine-Himalayan belt between eastern Turkey and Caucasus, *Geophys. J. R. astr. Soc.,* **77,** 185–246.

Jackson, J.A. & McKenzie, D.P., 1988. The relationship between plate motions and seismic tensors, and the rates of active deformation in the Mediterranean and Middle East, *Geophys. J. R. astr. Soc.,* **93,** 45–73.

Jackson, J.A., Haines, J. & Holt, W., 1995. The accommodation of the Arabia-Eurasia plate convergence in Iran, *J. geophys. Res.,* **100,** 15 205–15 219.

Jacob, K.H. & Quittmeyer, R.L., 1979. The Makran region of Pakistan and Iran: Trench-arc system with active plate subduction, in *Geodynamics of Pakistan,* pp. 305–317, eds Farah, A. & de Jong, K.A., Geological Survey of Pakistan, Quetta.

King, R.W. & Bock, Y., 2002. Documentation of the GAMIT GPS analysis software release 10.0, Mass. Inst. of Technol., Cambridge.

Kopp, C., Fruehn, J., Flueh, E.R., Reichert, C., Kukowski, N., Bialas, J. & Klaeschen, D., 2000. Structure of the Makran subduction zone from wide-angle and reflection seismic data, *Tectonophysics,* **329,** 171–191.

Masson, F., Anvari, M., Djamour, Y., Walpersdorf, A., Tavakoli, F., Daignieres, M., Nankali, H. & Van Gorp, S., 2007. Large-scale velocity field and strain tensor in Iran inferred from GPS measurements: new insight for the present-day deformation pattern within NE Iran, *Geophys. J. Int.,* **170,** 436–440.

Massonnet, D. & Feigl, K., 1998. Radar interferometry and its application to changes in the earth's surface, *Rev. Geophys.,* **36**(4), 441–500.

Matsu'ura, M., Jackson, D.D. & Cheng, A., 1986. Dislocation model for aseismic crustal deformation at Hollister, California, *J. geophys. Res.,* **91,** 12 661–12 674.

McCaffrey, R., 1995. *DEF-NODE Users Guide,* Rensselaer Polytechnic Institute, Troy.

McCaffrey, R., 2002. Crustal block rotations and plate coupling, in *Plate Boundary Zones,* Vol. 30, pp. 101–122, eds Stein, S. & Freymueller, J., AGU Geodynamics Series.

McCall, G.J.H., 1997. The geotectonic history of the Makran and adjacent areas of southern Iran, *J. Asian Sci.,* **15,** 517–531.

McClusky, S., Reilinger, R., Mahmoud, S., Ben Sari, D. & Tealeb, A., 2003. GPS constraints on Africa (Nubia) and Arabia plate motions, *Geophys. J. Int.,* **155,** 126–138.

Meade, B.J. & Hager, B.H., 1999. Simultaneous inversions of geodetic and geologic data for block motions in plate boundary zones, *EOS, Trans. Am. Geophys. Un.*, Paper G51B-16.

Musson, R.M.W., 2009. Subduction in the Western Makran: the historian's contribution, *J. Geol. Soc., Lond.,* **166,** 387–391, doi:10.1144/0016–76492008-119.

Platt, J.P., Leggett, J.K., Young, J., Raza, H. & Adam, S., 1985. Large scale sediment underplating in the Makran accretionary prism, *Southwest Pakistan, Geol.,* **13,** 507–511.

Platt, J.P., Leggett, J.K. & Alam, S., 1988. Slip vectors and fault mechanics in the Makran accretionary wedge, Southwest Pakistan, *J. geophys. Res.,* **93,** 7955–7973.

Regard, V., Bellier, O., Thomas, J.-C., Abbassi, M.R., Mercier, J., Shabanian, E., Feghhi, K. & Soleymani, S., 2004. Accomodation of Arabia-Eurasia convergence in the Zagros-Makran transfer zone, SE Iran: a transition between collision and subduction through a young deforming system, *Tectonics,* **23,** TC4007, doi:10.1029/2003TC001599.

Regard, V. *et al.,* 2005. Cumulative right-lateral fault slip rate across the Zagros-Makran transfer zone: role of the Minab-Zendan fault system in accommodating Arabia-Eurasia convergence in southeast Iran, *Geophys. J. Int.,* **160,** 1–25.

Regard, V. *et al.,* 2008. The transition between Makran subduction and the Zagros collision: recent advances in its structure and active deformation, *J. Geol. Soc. Lond.,* Special Issue, 1-23.-hal-00356532.

Reilinger, R. *et al.,* 2006. GPS constraints on continental deformation in the Africa-Arabia-Eurasia continental collision zone and implications for the dynamics of plate interactions, *J. geophys. Res.,* **111,** B05411, doi:10.1029/2005JB004051.

Rosen, P.A., Henley, S., Peltzer, G. & Simons, M., 2004. Updated Repeat Orbit Interferometry Package Released, *EOS Trans. Am. Geophys. Un.,* **85**(5), 47.

Sandwell, D.T. & Price, E.J., 1998. Phase gradient approach to stacking interferograms, *J. geophys. Res.,* **103**(B12), 30 183–30 204.

Savage, J.C. & Burford, R.O., 1973. Geodetic determination of the relative plate motion in central California, *J. geophys. Res.,* **78,** 832–845.

Talebian, M. & Jackson, J., 2004. A reappraisal of earthquake focal mechanisms and active shortening in the Zagros mountains of Iran, *Geophys. J. Int.,* **156,** 506–526.

Tatar, M., Hatzfeld, D., Martinod, J., Walpersdorf, A., Ghafori-Ashtiany, M. & Chery, J., 2002. The present-day deformation of the central Zagros from GPS measurements, *Geophys. Res. Lett.,* **29,** doi:10.1029/2002GL015427.

Vernant, P. *et al.,* 2004. Present-day crustal deformation and plate kinematics in Middle East constrained by GPS measurements in Iran and northern Oman, *Geophys. J. Int.,* **157,** 381–398.

Walpersdorf, A. *et al.,* 2006. Difference in the GPS deformation pattern of North and Central Zagros (Iran), *Geophys. J. Int.,* **167,** 1077–1088.

White, R.S., 1982. Deformation of the Makran accretionary sediment prism in the Gulf of Oman (north-west Indian Ocean), in *'Trench and Fore-Arc Geology: Sedimentation and Tectonics on Modern and Ancient Active Plate Margins',* ed. Leggett, J.K., Blackwell Scientific Publications, Oxford.

Yamini-Fard, F., Hatzfeld, D., Farahbod, A.M., Paul, A. & Mokhtari, M., 2007. The diffuse transition between the Zagros continental collision and the Makran oceanic subduction (Iran): microearthquake seismicity and crustal structure, *Geophys. J. Int.,* **170,** 182–194.

Zebker, H.A. & Villasenor, J., 1992. Decorrelation in interferometric radar surface echoes, *IEEE Trans. Geosci. Remote Sens.,* **30**(5), 950–959.